J|A|C|S
ARTICLES
Published on Web 06/03/2006

Artificial Transfer Hydrogenases Based on the Biotin−(Strept)avidin Technology: Fine Tuning the Selectivity by Saturation Mutagenesis of the Host Protein

Christophe Letondor,[‡] Anca Pordea,[‡] Nicolas Humbert,[‡] Anita Ivanova,[‡] Sylwester Mazurek,[§] Marjana Novic,[§] and Thomas R. Ward*,[‡]

Contribution from the Institute of Chemistry, University of Neuchâtel, Av. Bellevaux 51, CP 2, CH-2007 Neuchâtel, Switzerland, and Laboratory of Chemometrics, National Institute of Chemistry, Hajdrihova 19, SI-1001 Ljubljana, Slovenia

Received March 7, 2006; E-mail: thomas.ward@unine.ch

Abstract: Incorporation of biotinylated racemic three-legged d^6-piano stool complexes in streptavidin yields enantioselective transfer hydrogenation artificial metalloenzymes for the reduction of ketones. Having identified the most promising organometallic catalyst precursors in the presence of wild-type streptavidin, fine-tuning of the selectivity is achieved by saturation mutagenesis at position S112. This choice for the genetic optimization site is suggested by docking studies which reveal that this position lies closest to the biotinylated metal upon incorporation into streptavidin. For aromatic ketones, the reaction proceeds smoothly to afford the corresponding enantioenriched alcohols in up to 97% ee (*R*) or 70% (*S*). On the basis of these results, we suggest that the enantioselection is mostly dictated by CH/π interactions between the substrate and the η^6-bound arene. However, these enantiodiscriminating interactions can be outweighed in the presence of cationic residues at position S112 to afford the opposite enantiomers of the product.

Introduction

The asymmetric reduction of C═O and C═N bonds is one of the most fundamental transformations in organic chemistry. Although efficient heterogeneous catalysts exist for such reductions,[1] homogeneous and enzymatic catalysts dominate this active field of investigation.[2,3] Both latter approaches have evolved independently and can achieve high levels of enantioselection for selected substrate classes.

With the aim of alleviating some of the inherent limitations of existing methodologies, two bio-inspired approaches have recently witnessed a revival: (i) organocatalysis[4,5] and (ii) artificial metalloenzymes.[6−8]

(i) Originally developed in the late 1960s,[9,10] metal-free catalytic systems (organocatalysts), sometimes referred to as minimal enzymes, have found numerous applications in the past decade. In recent months, significant advances in the context of enantioselective organocatalytic reduction of imines and ketones have been published.[11−13]

(ii) Initially proposed by Kaiser[14] and Whitesides[15] in the late 1970s, artificial metalloenzymes based on either a covalent[16−18] or a supramolecular anchoring[19−23] of an organometallic catalyst precursor in a macromolecular host (protein or DNA[24]), are gaining attention in the context of enantioselective catalysis.[25]

In terms of catalyst performance, artificial metalloenzymes offer the appealing prospect of a combined chemogenetic optimization: the host protein can be optimized by genetic means, and the organometallic catalyst precursor can be chemically modified. In the spirit of enzymes, such hybrid catalysts provide a well-defined chiral second coordination sphere. By incorporating an achiral or racemic organometallic

‡ University of Neuchâtel.
§ National Institute of Chemistry.

(1) Bürgi, T.; Baiker, A. *Acc. Chem. Res.* **2004**, *37*, 909−917.
(2) Jacobsen, E. N.; Pfaltz, A.; Yamamoto, H. *Comprehensive Asymmetric Catalysis*; Springer: Berlin, 1999.
(3) Faber, K. *Biotransformations in Organic Chemistry*. 5th ed.; Springer: Berlin, 2004.
(4) Berkessel, R.; Gröger, H. *Metal-free organic catalysts in asymmetric synthesis*; Wiley-VCH: Weinheim, 2005.
(5) Dalko, P. I.; Moisan, L. *Angew. Chem., Int. Ed.* **2004**, *43*, 5138−5175.
(6) Qi, D.; Tann, C.-M.; Haring, D.; Distefano, M. D. *Chem. Rev.* **2001**, *101*, 3081−3111.
(7) Thomas, C. M.; Ward, T. R. *Chem. Soc. Rev.* **2005**, *34*, 337−346.
(8) Davis, B. G. *Curr. Opin. Biotechnol.* **2003**, *14*, 379−386.
(9) Pracejus, H.; Mätje, H. *J. Prakt. Chem.* **1964**, *24*, 195−205.
(10) Eder, U.; Sauer, G.; Wiechert, R. *Angew. Chem., Int. Ed. Engl.* **1971**, *10*, 496−497.
(11) Akiyama, T.; Morita, H.; Itoh, J.; Fuchibe, K. *Org. Lett* **2005**, *7*, 2583−2585.
(12) Hoffmann, S.; Seayad, A. M.; List, B. *Angew. Chem., Int. Ed.* **2005**, *44*, 7424−7427.
(13) Malkov, A. V.; Liddon, A. J. P. S.; Ramirez-Lopez, P.; Bendova, L.; Haigh, D.; Kocovsky, P. *Angew. Chem., Int. Ed.* **2006**, *45*, 1432−1435.
(14) Kaiser, E. T.; Lawrence, D. S. *Science* **1984**, *226*, 505−511.
(15) Wilson, M. E.; Whitesides, G. M. *J. Am. Chem. Soc.* **1978**, *100*, 306−307.
(16) Panella, L.; Broos, J.; Jin, J.; Fraaije, M. W.; Janssen, D. B.; Jeronimus-Stratingh, M.; Feringa, B. L.; Minnaard, A. J.; de Vries, J. G. *Chem. Commun.* **2005**, *5656−5658*.
(17) Carey, J. R.; Ma, S. K.; Pfister, T. D.; Garner, D. K.; Kim, H. K.; Abramite, J. A.; Wang, Z.; Guo, Z.; Lu, Y. *J. Am. Chem. Soc.* **2004**, *126*, 10812−10813.
(18) Kruithof, C. A.; Casado, M. A.; Guillena, G.; Egmond, M. R.; van der Kerk-van Hoof, A.; Heck, A. J. R.; Klein Gebbink, R. J. M.; van Koten, G. *Chem. Eur. J.* **2005**, *11*, 6869−6877.
(19) Okrasa, K.; Kazlauskas, R. J. *Chem. Eur. J.* **2006**, *12*, 1587−1596.
(20) Mahammed, A.; Gross, Z. *J. Am. Chem. Soc.* **2005**, *127*, 2883−2887.
(21) Lin, C.-C.; Lin, C.-W.; Chan, A. S. C. *Tetrahedron Asymmetry* **1999**, *10*, 1887−1893.
(22) Ohashi, M.; Koshiyama, T.; Ueno, T.; Yanase, M.; Fujii, H.; Watanabe, Y. *Angew. Chem., Int. Ed.* **2003**, *42*, 1005−1008.
(23) Reetz, M. T.; Jiao, N. *Angew. Chem., Int. Ed.* **2006**, *45*, 2416−2419.
(24) (a) Roelfes, G.; Feringa, B. L. *Angew. Chem., Int. Ed.* **2005**, *44*, 3230−3232. (b) Roelfes, G.; Boersma, A. J.; Feringa, B. L. *Chem. Commun.* **2006**, 635−637.
(25) Krämer, R. *Angew. Chem., Int. Ed.* **2005**, *45*, 858−860.

10.1021/ja061580o CCC: $33.50

moiety within a chiral protein scaffold, the influence of the second coordination sphere on enantioselectivity can be addressed.

In the context of artificial metalloenzymes based on the biotin−(strept)avidin technology, we recently demonstrated the versatility of such a chemogenetic optimization for the enantioselective hydrogenation of *N*-protected dehydroamino acids.[26−28]

As a second catalytic transformation to implement in this context, we focus on the transfer hydrogenation of ketones catalyzed by d^6-piano stool complexes.[29−36] This choice is motivated by:

(i) the theoretical suggestion that this reaction proceeds without coordination of the substrate to the metal.[38−41] The chiral recognition pattern for this organometallic transformation is thus reminiscent of enzymatic catalysis. Indeed, the second coordination sphere provided by an enzyme is optimized to steer the enantiodiscrimination step without necessarily requiring covalent (or dative) binding of the substrate to the enzyme. The general concept of this approach is depicted in Scheme 1.

(ii) the compatibility between d^6-piano stool complexes and enzymes at elevated temperatures, as established by Bäckvall in the context of dynamic kinetic resolution of alcohols via acylation.[37]

We reasoned that, as the substrate does not bind to the metal center during the transfer hydrogenation (Scheme 1), a well-defined second coordination sphere provided by the host protein around a piano stool complex offers an attractive means to optimize the selectivity of transfer hydrogenation catalysts.

The starting point for the present work was the identification of [η^6-(arene)Ru(**Biot**−***q*-L**)Cl] (q = ortho, meta, para, see Scheme 4) complexes as active and selective catalyst precursors for the transfer hydrogenation of acetophenone derivatives. In the presence of various streptavidin mutants, we recently reported on enantioselectivities > 90% for the reduction of *p*-methylacetophenone.[32]

With the aim of broadening the substrate scope and gaining mechanistic insight, we screened 20 streptavidin isoforms in combination with 21 biotinylated d^6-piano stool complexes.

Results and Discussion

Docking Studies. To shed light on the localization of the biotinylated three-legged piano stool catalyst, docking studies were performed using AutoDock 3.0.5.[42,43] All docking simulations presented below are based on a rigid host model and thus should be considered as qualitative. Computational details can be found in the Supporting Information.

Scheme 1. Artificial Metalloenzymes Based on Biotin−Streptavidin for Enantioselective Transfer Hydrogenation Reactions[a]

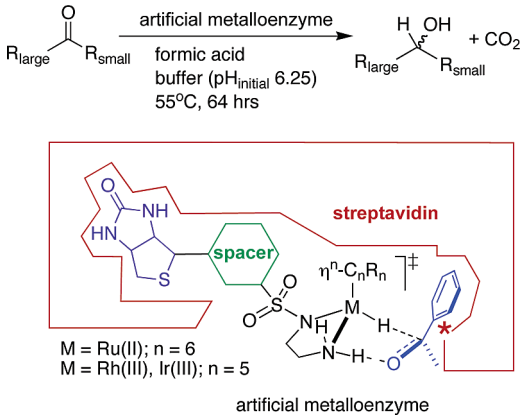

[a] The host protein (streptavidin, red) displays a high affinity for the anchor (biotin, violet); introduction of a spacer (green) and variation of the metal and the η^n-bond arene (black) allows one to chemically optimize the activity and the selectivity. Saturation mutagenesis (red star) allows a genetic optimization of the host protein. In the transition state of the transfer hydrogenation, both hydrogens are delivered to the prochiral substrate (blue) without the substrate coordinating to the metal.

Since tetrameric wild-type streptavidin (abbreviated hereafter WT Sav) consists of a dimer of dimer with two proximal and two distal binding sites, docking studies were carried out on the dimeric structure (with two proximal binding sites: A and C subunits) downloaded from the protein data bank (http://www.rcsb.org/pdb/): 1stp for streptavidin.[44] Following the docking procedure, the B and D subunits of streptavidin were included for the computation of distances.

The biotinylated complexes [η^6-(arene)Ru(**Biot**−***p*-L**)H] (arene = *p*-cymene, benzene) were built using Hyperchem 7.5 based on the structurally characterized [η^6-(*p*-cymene)Ru(Tos-DPEN)-Cl] (Tos-DPEN: (*R*,*R*)-*p*-tolylsulfonamido-diphenyl-ethylene-diamine, CSD code: TAXFON)[45] as well as the (+)-biotin anchor extracted from 1stp. For docking purposes, the (*Z*)-configuration of the amide was enforced (Scheme 2 in red) and the geometry around ruthenium was frozen. Both (*R*)- and (*S*)-configurations at ruthenium were considered, and the dihedral angle around amidic C−C bond was set to $\tau = 0°$ and 180° (Scheme 2, in violet), thus yielding a total of four different isomers which were docked in streptavidin.[46] The energy minimization was performed by allowing rotation around the bonds highlighted in green in Scheme 2.

To estimate the quality of the docking procedure, biotin and the docked [η^6-(arene)Ru(**Biot**−***p*-L**)H] were superimposed in streptavidin, and the root-mean-square error values (rms) were

(26) Skander, M.; Humbert, N.; Collot, J.; Gradinaru, J.; Klein, G.; Loosli, A.; Sauser, J.; Zocchi, A.; Gilardoni, F.; Ward, T. R. *J. Am. Chem. Soc.* **2004**, *126*, 14411−14418.
(27) Klein, G.; Humbert, N.; Gradinaru, J.; Ivanova, A.; Gilardoni, F.; Rusbandi, U. E.; Ward, T. R. *Angew. Chem., Int. Ed.* **2005**, *44*, 7764−7767.
(28) Collot, J.; Gradinaru, J.; Humbert, N.; Skander, M.; Zocchi, A.; Ward, T. R. *J. Am. Chem. Soc.* **2003**, *125*, 9030−9031.
(29) Schlatter, A.; Kundu, M. K.; Woggon, W.-D. *Angew. Chem., Int. Ed.* **2004**, *43*, 6731−6734.
(30) Noyori, R.; Hashiguchi, S. *Acc. Chem. Res.* **1997**, *30*, 97−102.
(31) Clapham, S. E.; Hadzovic, A.; Morris, R. H. *Coord. Chem. Rev.* **2004**, *248*, 2201−2237.
(32) Letondor, C.; Humbert, N.; Ward, T. R. *Proc. Natl. Acad. Sci. U.S.A.* **2005**, *102*, 4683−4687.
(33) Reetz, M. T.; Li, X. *J. Am. Chem. Soc.* **2006**, *128*, 1044−1045.
(34) Palmer, M. J.; Wills, M. *Tetrahedron Asymmetry* **1999**, *10*, 2045−2061.
(35) Blaser, H.-U.; Malan, C.; Pugin, B.; Spindler, F.; Steiner, H.; Studer, M. *Adv. Synth. Catal.* **2003**, *345*, 103−151.
(36) Wu, X.; Vinci, D.; Ikariya, T.; Xiao, J. *Chem. Commun.* **2005**, 4447−4449.
(37) Pàmies, O.; Bäckvall, J.-E. *Chem. Rev.* **2003**, *103*, 3247−3261.
(38) Muniz, K. *Angew. Chem., Int. Ed.* **2005**, *44*, 6622−6627.
(39) Yamakawa, M.; Ito, H.; Noyori, R. *J. Am. Chem. Soc.* **2000**, *122*, 1466−1478.
(40) Yamakawa, M.; Yamada, I.; Noyori, R. *Angew. Chem., Int. Ed.* **2001**, *40*, 2818−2821.
(41) Brandt, P.; Roth, P.; Andersson, P. G. *J. Org. Chem.* **2004**, *69*, 4885−4890.
(42) Morris, G. M.; Goodsell, D. S.; Halliday, R. S.; Huey, R.; Hart, W. E.; Belew, R. K.; Olson, A. J. *J. Comput. Chem.* **1998**, *19*, 1639−1662.
(43) Goodsell, D. S.; Morris, G. M.; Olson, A. J. *J. Mol. Recognit.* **1996**, *9*, 1−5.
(44) Weber, P. C.; Ohlendorf, D. H.; Wendoloski, J. J.; Salemme, F. R. *Science* **1989**, *243*, 85−88.
(45) Uematsu, N.; Fujii, A.; Hashiguchi, S.; Ikariya, T.; Noyori, R. *J. Am. Chem. Soc.* **1996**, *118*, 4916−4917.
(46) Cornell, W. D.; Cieplak, P.; Bayly, C. I.; Gould, I. R.; Merz, K. M., Jr; Ferguson, D. M.; Spellmeyer, D. C.; Fox, T.; Caldwell, J. W.; Kollman, P. A. *J. Am. Chem. Soc.* **1995**, *117*, 5179−5197.

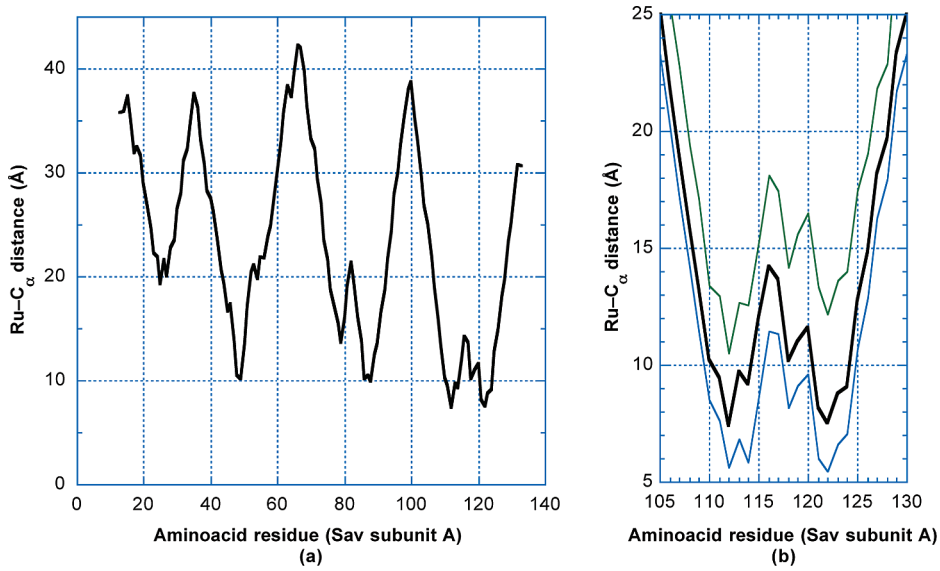

Figure 1. Computed average Ru−Cα distances for [η^6-(*p*-cymene)Ru(**Biot**−***p*-L**)H] ⊂ WT Sav resulting from the 135 docking simulations with rms < 1 Å (a); zoom-in of the critical L7,8 Ru−Cα loop distances including shortest and longest Ru−Cα distances computed for the 135 docking simulations (blue and green lines respectively) (b).

Scheme 2. Structure and Variable Parameters of [η^6-(*p*-cymene)Ru((**Biot**−***p*-L**)H] Used for the Docking Studies[a]

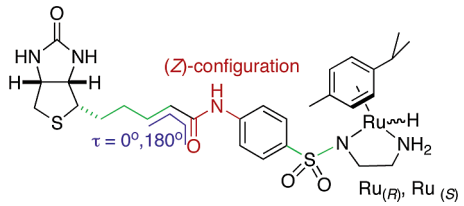

[a] The dihedral angle (purple) was set to $\tau = 0°$ and 180°, the absolute configuration at ruthenium was set to (*R*) and (*S*) thus yielding a total of four isomers used for the docking in dimeric streptavidin; rotation around the bonds highlighted in green was allowed during the energy minimization procedure.

determined for biotin's bicyclic scaffold. Only the structures with an rms < 1 Å were retained for further analysis.

Fifty runs were performed for each of the four [η^6-(*p*-cymene)Ru(**Biot**−***p*-L**)H] isomers ((*R*)- *and* (*S*)- configurations at Ru and $\tau = 0°$ and 180°), yielding a total of 200 docked structures [η^6-(*p*-cymene)Ru(**Biot**−***p*-L**)H] ⊂ WT Sav. Following the docking in dimeric streptavidin, the complete tetrameric host was redisplayed. For the docked structures with rms < 1 Å (135 in total), the Ru−Cα distances (Cα is the asymmetric carbon of each amino acid residue in the tetrameric streptavidin) were computed and are displayed in Figure 1. For the other B, C, and D subunits, only one Ru−Cα contact shorter than 10 Å was computed (with Lys 121, subunit C, 9.42 Å).

From the Ru−Cα distances, it appears that only two amino acid residues display an average distance Ru−Cα < 8 Å. These are: S112, S122, both part to the L 7,8 loop of subunit A of streptavidin, in which the [η^6-(*p*-cymene)Ru(**Biot**−***p*-L**)H] was docked. For the S112- and the S122 residues, the computed average Ru−Cα distances are 7.41 and 7.51 Å with standard deviations (SD) = 0.91 Å and SD = 1.43 Å respectively. The extreme distances displayed as green and blue lines in Figure 1b thus overemphasize the scattering of the calculated Ru−Cα distances for a particular set of docking simulations. A histogram of the distances for both S112- and S122 residues is provided in the Supporting Information. For the η^6-bound arene, three C−Cα distances <8 Å are computed with residue S112. This suggests that there may be significant interactions between the side chain amino acid residue at this position and the η^6-bound arene.

The structure of the most stable [η^6-(*p*-cymene)Ru(**Biot**−***p*-L**)H] ⊂ WT Sav is presented in Figure 2. As can be appreciated, the ruthenium moiety (ball-and-stick representation) is embedded within a cavity provided by monomers A, B, and C of streptavidin (green, yellow, and blue solvent accessible surfaces). In this supramolecular assembly [η^6-(*p*-cymene)Ru(**Biot**−***p*-L**)H] ⊂ WT Sav, the catalytic moiety remains well accessible to an incoming prochiral substrate.

The two closest lying amino acid residues, S112 and S122, are highlighted (red and blue stick representation). The modeled structure shows that the S112 side chain points toward the piano stool moiety, whereas the S122 side chain points away. As a consequence, the computed serine oxygens are repectively 5.61 and 9.15 Å away from the ruthenium center. Very similar qualitative results are obtained for [η^6-(benzene)Ru(**Biot**−***p*-L**)H] ⊂ WT Sav.[47]

In the absence of precise structural information, we assume that mutations close to the active site bring more diversity than distant mutations.[48] With the aim of steering the delivery of the incoming prochiral substrate, we favored position S112 over S122 for saturation mutagenesis as its side chain points toward the ruthenium.

Screening Strategy. To generate diversity, we combine chemical- with genetic optimization strategies. Combining *m* streptavidin isoforms with *n* biotinylated catalyst precursors yields a two-dimensional diversity matrix of *n*·*m* experiments.

In our previous study on artificial metalloenzymes for the hydrogenation of *N*-protected dehydroamino acids, we estab-

(47) It is interesting to note that the amino acid P64 of subunit B (yellow stick representation, average Ru−Cα distance 15.15 Å) is within van der Waals contact of the loop L7,8 (which contains residues 112−122) of subunit A of streptavidin. This observation suggests that the P64G mutation may act via a relay mechanism: influencing the L7,8 loop, which in turn, affects the chiral discrimination event with [η^6-(arene)Ru(**Biot**−***p*-L**)H] ⊂ P64G Sav.

(48) Morley, K. L.; Kazlauskas, R. J. *Trends Biotechnol.* **2005**, *23*, 231−237.

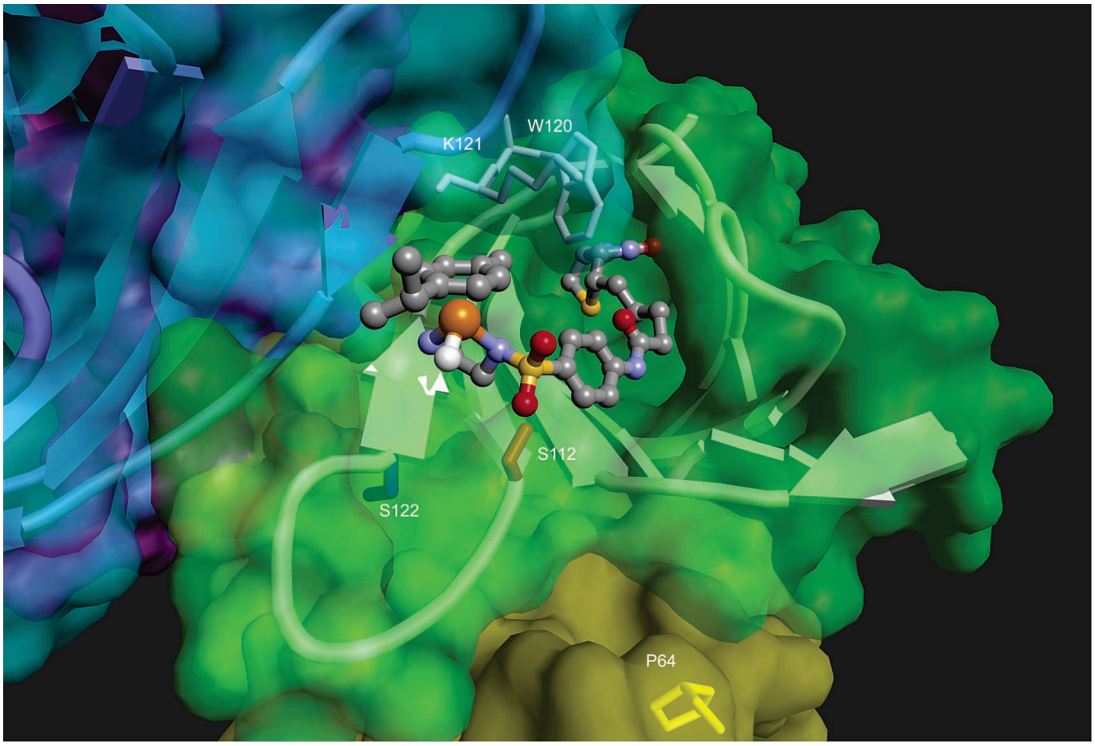

Figure 2. Result of the docking simulation between [η^6-(*p*-cymene)Ru(**Biot**−***p*-L**)H] (ball-and-stick representation) and WT streptavidin (transparent green, blue, yellow, and violet for solvent accessibility in subunits A, B, C, and D respectively and schematic secondary structure for A and C subunits). Close lying S112 and S122 residues are highlighted (red and blue stick representations respectively), residues P64 (subunit B, yellow stick representation), W120 (subunit C, white stick representation), the hydrophobic lid which shields the biotin binding site of subunit A as well as K121 (subunit C, white stick representation).

lished that the chemical optimization brings more diversity than the genetic counterpart.[27] To reduce the number of screening experiments, we opted for a representational search strategy[49] to optimize the selectivity of the artificial metalloenzymes.

In a first screening round, all 21 catalyst precursors were evaluated in combination with two streptavidin isoforms. For the second round, the most promising biotinylated catalysts were screened with the 20 streptavidin isoforms derived from saturation mutagenesis at position S112. Finally, the best catalyst ⊂ protein combinations were tested with different ketones to evaluate the substrate scope of the artificial metalloenzymes. This optimization strategy is sketched in Figure 3. The substrates and their corresponding reduction products used in this study are depicted in Scheme 3.

Buffer-screening experiments revealed that the initial pH is critical both for the activity and for the selectivity of the artificial transfer hydrogenases.[50−52] The pH-dependence profile for the reduction of acetophenone is depicted in Figure 4. As the conversion increases sharply between pH 6.0−6.5 at the cost of a modest erosion of enantioselectivity, we set the $pH_{initial}$ = 6.25. Combining sodium formate (pK_a = 3.75) with boric acid (pK'_a = 9.24) affords an acid−base mixture which, at its isoelectric point, displays a pH = 0.5·(pK_a + pK'_a) = 6.50. Using a 0.48 M $NaHCO_2$ combined with 0.41 M boric acid yields a solution with pH = 6.25. However, as this mixture

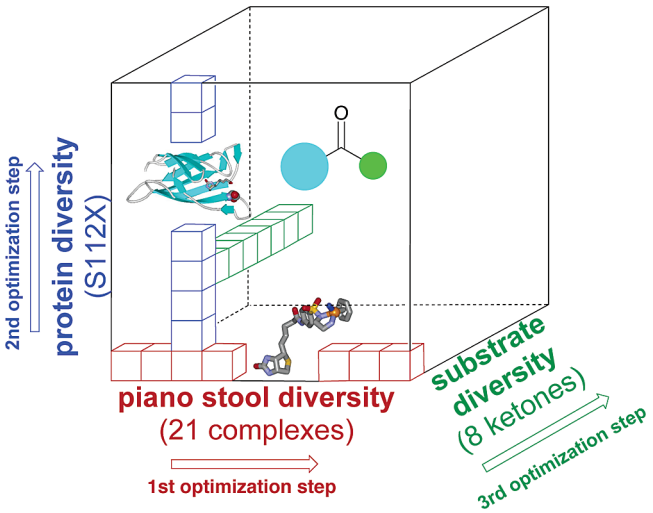

Figure 3. Representational search strategy[49] allowing a rapid identification of good catalyst ⊂ protein combinations without examination of all possibilities.

possesses no buffering capacity at this pH, the pH rises sharply during catalysis, resulting from formate dehydrogenase activity of the catalyst. Addition of MOPS (3-(*N*-morpholino)propanesulfonic acid sodium salt, 0.16 M) allows one to maintain the pH < 7.3 ($pH_{initial}$ = 6.25) throughout catalysis.

Genetic Diversity. Saturation mutagenesis was carried out according to the quick-change mutagenesis protocol using the degenerate NNS codons at position S112. Due to the abundance of G·C base pairs in the Sav gene, the polymerase chain reaction (PCR) conditions were adapted to ensure proper amplification of the gene. The optimized PCR conditions are: 5% DMSO,

(49) Shimizu, K. D.; Snapper, M. L.; Hoveyda, A. H. *Chem. Eur. J.* **1998**, *4*, 1885−1889.
(50) Wu, X.; Li, X.; Hems, W.; King, F.; Xiao, J. *Org. Biomol. Chem.* **2004**, *2*, 1818−1821.
(51) Ogo, S.; Abura, T.; Watanabe, Y. *Organometallics* **2002**, *21*, 2964−2969.
(52) Wu, X.; Li, X.; King, F.; Xiao, J. *Angew. Chem., Int. Ed.* **2005**, *44*, 3407−3411.

Scheme 3. Substrates and Reduction Products Used in This Study[a]

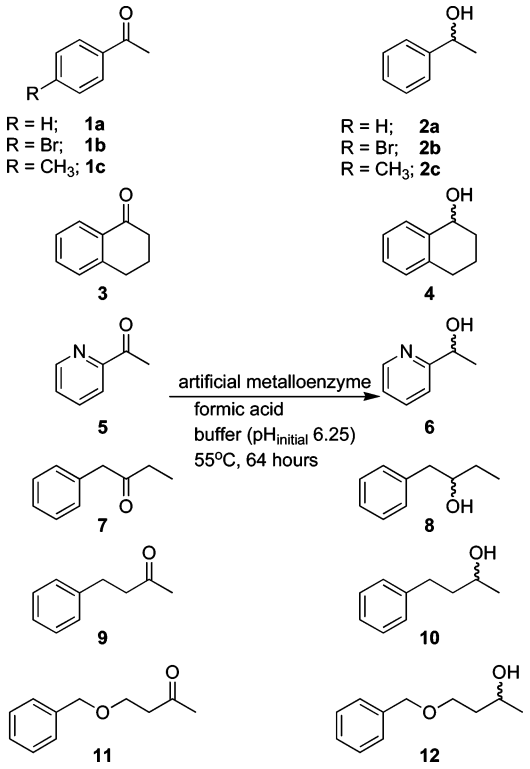

[a] Cocktail compositions: **1a, 1b** and **1c**; **5** and **7**; **9** and **11**. α-tetralone **3** was screened individually.

DNA denaturated at 95 °C for 5 min, followed by 16 cycles (denaturation at 95 °C, 1 min; primer hybridization 65 °C, 1 min; DNA polymerization 68 °C, 15 min). A final elongation (65 °C, 1 h) completed the PCR.

All 20 S112X Sav isoforms could be isolated and purified by iminobiotin affinity chromatography, thus demonstrating the biotin-binding capability of the mutants.[53]

Chemical Diversity. A total of 21 biotinylated d^6-piano stool complexes [η^n-(arene)M(**Biot**−***q*-L**)Cl] (η^n-arene = η^6-*p*-cymene, η^6-benzene, η^6-mesitylene, η^6-durene, η^6-hexamethylbenzene, η^5-pentamethylcyclopentadienyl; M = Ru(II), Ir(III), and Rh(III); *q* = *ortho*-, *meta*-, and *para*-) were prepared in situ by reacting [η^n-(arene)MCl_2]$_2$ with the appropriate ligand in refluxing 2-propanol in the presence of NEt_3 (Scheme 4).

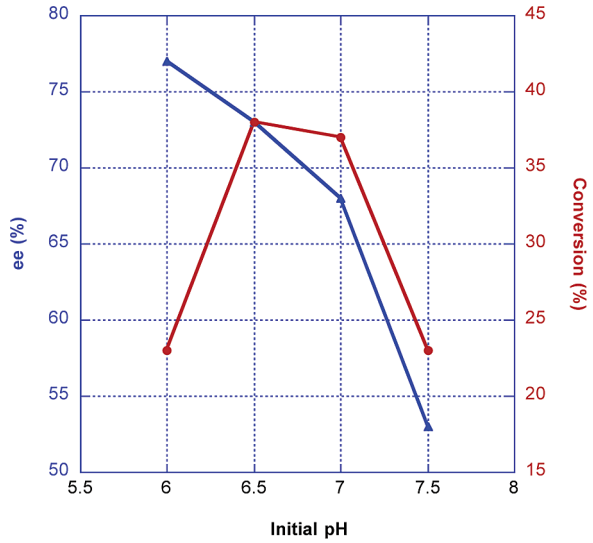

Figure 4. pH-dependence profile of the activity (red circles) and of the selectivity (blue triangles) for the reduction of acetophenone **1a** with [η^6-(*p*-cymene)Ru(**Biot**−***p*-L**)H] ⊂ WT Sav.

Complete experimental details for the ligand synthesis as well as the catalytic runs are compiled in the Supporting Information.

For the first optimization step, the 21 catalyst precursors [η^n-(C_nR_n)M(**Biot**−***q*-L**)Cl] were screened in the presence of WT Sav as well as P64G Sav. This mutant was selected as [η^6-(*p*-cymene)Ru(**Biot**−***p*-L**)Cl] ⊂ P64G Sav had previously been identified as the best mutant for the enantioselective reduction of *p*-methylacetophenone **1c**.[32] To accelerate the optimization process, a cocktail containing three aromatic substrates (acetophenone **1a**, *p*-bromoacetophenone **1b**, and *p*-methylacetophenone **1c**) were screened simultaneously using a 3 mol % catalyst loading (i.e. 11 equiv of each substrate vs Ru). Control experiments established that the selectivity and the conversion obtained with this cocktail are similar, but not always identical, to those obtained with a single substrate (i.e., small autoinduction).[54]

The results of the screening experiments with all three substrates are summarized in Figure 5 using a fingerprint display for each substrate−protein−ligand combination.[27,55] The selectivity is color-coded: strawberry for (*S*)-selective and green for (*R*)-selective ligand−protein combinations.[56] The intensity of the color reflects the conversion. This convenient display allows

Scheme 4. Chemical Diversity Generated by Combining [Cp*RhCl]-, [Cp*IrCl]- or [η^6-(arene)RuCl] Fragments with (**Biot**−***p*-L**) (*q*- = *ortho*-, *meta*- and *para*-)

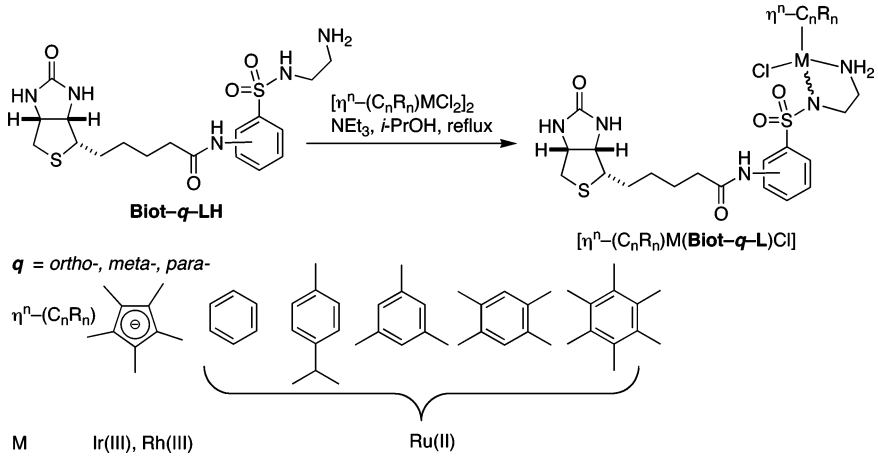

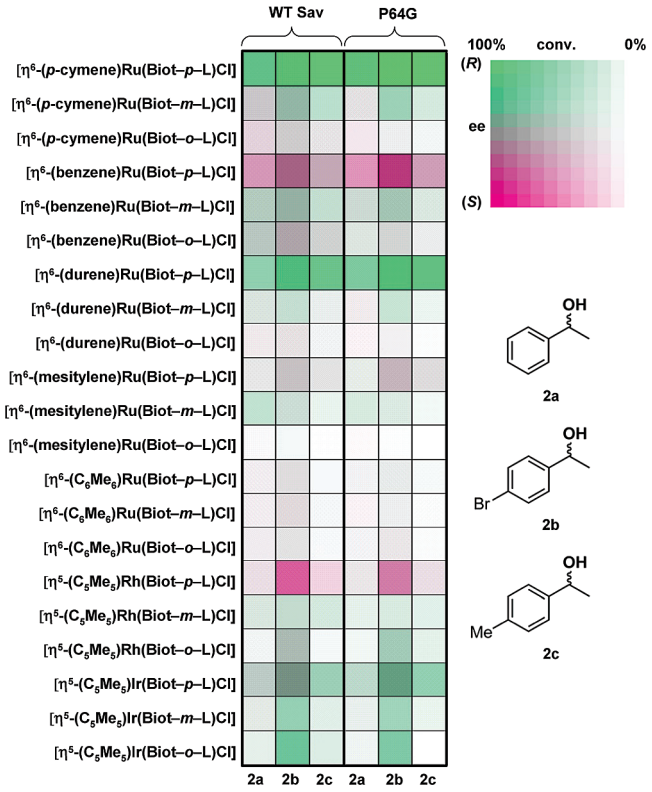

Figure 5. Fingerprint display of the results for the chemical optimization of the transfer hydrogenation of a cocktail containing acetophenone **1a**, *p*-bromoacetophenone **1b** and *p*-methylacetophenone **1c** in the presence of 21 biotinylated d^6-piano stool complexes [η^n-(arene)M(**Biot**−***q*-L**)Cl] with either WT Sav or P64G Sav as host proteins. The catalytic runs were performed at 55 °C for 40 h using the mixed buffer HCO_2Na (0.48 M) + $B(OH)_3$ (0.41 M) + MOPS (0.16 M) at $pH_{initial}$ = 6.25. Ru: substrates **1a**−**c**: formate ratio 1:33:4000 (i.e. 11 equiv of each substrate vs Ru). Please refer to the Supporting Information for a tabulation of all catalytic runs.

rapid identification of interesting ligand−protein combinations. Several interesting features are apparent from these data:

(i) Only catalyst precursors bearing a para-substituted aminosulfonamide **Biot**−***p*-L** afford any significant levels of reduction products.

(ii) The nature of the η^n-(arene) plays a critical role in determining both the activity and the selectivity of the corresponding hybrid catalysts. Although the [η^6-(mesitylene)Ru(**Biot**−***p*-L**)Cl] is a poor catalyst, the [η^6-(durene)Ru(**Biot**−***p*-L**)Cl] rivals with the best catalyst [η^6-(*p*-cymene)Ru(**Biot**−***p*-L**)Cl].

(iii) Although P64G Sav was previously identified as the best host protein in terms of enantioselectivity, both WT Sav and P64G Sav show similar trends.[32]

(iv) The most activated bromoketone **1b** gives the highest conversions. In general, the bulkier ketones **1b** and **1c** give the best enantioselectivity.

On the basis of this initial screening, we selected five biotinylated piano stool complexes for the genetic optimization with S112X mutants: [η^6-(*p*-cymene)Ru(**Biot**−***p*-L**)Cl] ((*R*)-selective, good conversions) > [η^6-(durene)Ru(**Biot**−***p*-L**)Cl] ((*R*)-selective, good conversions) > [η^6-(benzene)Ru(**Biot**−***p*-L**)Cl] ((*S*)-selective, moderate conversions) > [η^5-(C_5Me_5)Rh(**Biot**−***p*-L**)Cl] ((*S*)-selective, moderate conversions) > [η^5-(C_5Me_5)Ir(**Biot**−***p*-L**)Cl] ((*R*)-selective, moderate conversions).

These five complexes were combined with the 19 mutants resulting from saturation mutagenesis at position S112X Sav. The results of the cocktail screening are displayed in a fingerprint format in Figure 6. For convenience, the column vectors are arranged according to the amino acid properties at position 112. To refine the trends observed in the fingerprint display (Figure 6), enantioselectivity histograms are displayed for five representative S112X mutants and for the five complexes in Figure 7a and b, respectively. Table 1 summarizes the results of the best catalytic runs, which were reproduced with a single substrate and a 1 mol % catalyst loading (i.e. 100 equiv of substrate vs Ru).

The general trends that emerge from this chemogenetic optimization can be summarized as follows:

(i) Both the [η^6-(*p*-cymene)Ru(**Biot**−***p*-L**)Cl] and the [η^6-(durene)Ru(**Biot**−***p*-L**)Cl] complexes exert a strong prefence in favor of the (*R*)-products (ee > 85% (*R*) in 9 cases, Table 1, entries 1−5). This propensity can be partially overruled in the presence of cationic residues at position S112, favoring (*S*)-products with modest conversions and selectivity (up to 20(*S*) % ee, Table 1 entry 6). Thus, using [η^6-(*p*-cymene)Ru(**Biot**−***p*-L**)Cl], introduction of a single point mutation at position S112 can afford reduction product with differences in enantioselectivity $\Delta ee < 110\%$. This corresponds to differences in transition-state free energies $\delta\Delta G^{\ddagger} < 1.99$ kcal·mol^{-1} at room temperature.

(ii) Altough less pronounced, [η^6-(benzene)Ru(**Biot**−***p*-L**)-Cl] favors mostly the (*S*)-enantiomers (Figure 7b). However, certain mutations at position S112 (S112F Sav, S112Y Sav, S112A Sav) can overrule this preference (Table 1, entry 7).

(iii) The selectivities of the [η^5-(C_5Me_5)Rh(**Biot**−***p*-L**)Cl]- and [η^5-(C_5Me_5)Ir(**Biot**−***p*-L**)Cl]-containing artificial metalloenzymes depend very much on the host protein. For the reduction of bromoketone **1b** using [η^5-(C_5Me_5)Rh(**Biot**−***p*-L**)-Cl], the S112F Sav and S112G Sav afford (*R*)-product (73% conversion, 60% ee) and (*S*)-product (60% conversion, 52% ee), respectively (Table 1, entries 8−9).

(iv) The conversion decreases with increasing steric bulk at position S112X Sav. For example: S112A > S112I ≈ S112L; S112N > S112Q; S112F > S112W.

(v) Potentially coordinating amino acid residues at position S112 (i.e. S112C, S112D, S112E, and S112H and to a lesser extent S112M) shut off the catalytic activity. This observation supports the docking simulations which suggest that the S112X side chain indeed lies close to the [M(**Biot**−***p*-L**)]-moiety.

(vi) Overall, the Ru catalysts outperform the Ir and Rh analogues both in terms of activity and of selectivity.

Having identified the most efficient biotinylated d^6-piano stool ⊂ S112X Sav mutant, we proceeded to test different substrates. For this purpose, we selected the sterically constrained aryl ketone α-tetralone **3**, 2-acetylpyridine **5**, and three dialkyl ketones **7**, **9**, and **11**. These five substrates were screened with both [η^6-(*p*-cymene)Ru(**Biot**−***p*-L**)Cl] and [η^6-(benzene)Ru-(**Biot**−***p*-L**)Cl] in the presence of representative Sav mutants: S112G, S112A, S112L (aliphatic residues with increasing bulk); S112F and S112W (aromatic residues with increasing bulk);

(53) Humbert, N.; Zocchi, A.; Ward, T. R. *Electrophoresis* **2005**, *26*, 47−52.
(54) Satyanarayana, T.; Kagan, H. B. *Adv. Synth. Catal.* **2005**, *347*, 737−748.
(55) Wahler, D.; Badalassi, F.; Crotti, P.; Reymond, J.-L. *Chem. Eur. J.* **2002**, *8*, 3211−3228.
(56) To generate the RGB codes for a catalytic experiment yielding one of the products in *x*% yield and *y*%(*R*) and z%(*S*) (100% − *y*% = *z*% (*S*)) the following formulas were implemented in an Excel Macro: RGB1 = [100 − (*y*·*x*)/100]·2.55; RGB2 = [100 − (*z*·*x*)/100]·2.55; RGB3 = 0.5·(RGB1+RGB2).

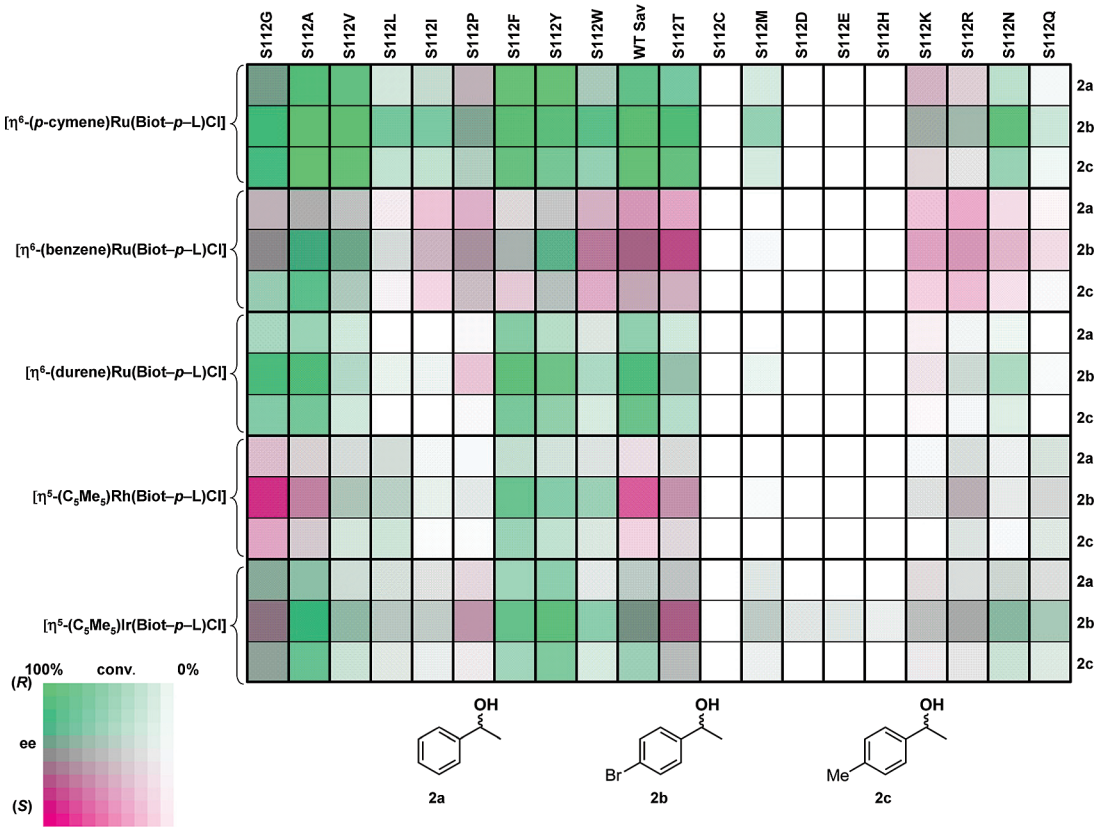

Figure 6. Fingerprint display of the results for the genetic optimization of the transfer hydrogenation of a cocktail containing acetophenone **1a**, *p*-bromoacetophenone **1b** and *p*-methylacetophenone **1c** in the presence of five biotinylated d^6-piano stool complexes [η^n-(arene)M(**Biot**−***p*-L**)Cl] combined with the 20 streptavidin isoforms S112X Sav. The catalytic runs were performed at 55 °C for 40 h using the mixed buffer HCO_2Na (0.48 M) + $B(OH)_3$ (0.41 M) + MOPS (0.16 M) at $pH_{initial}$ = 6.25. Ru: substrates **1a**−**c**: formate ratio 1:33:4000 (i.e. 11 equiv of each substrate vs Ru). Please refer to the Supporting Information for a tabulation of all catalytic runs.

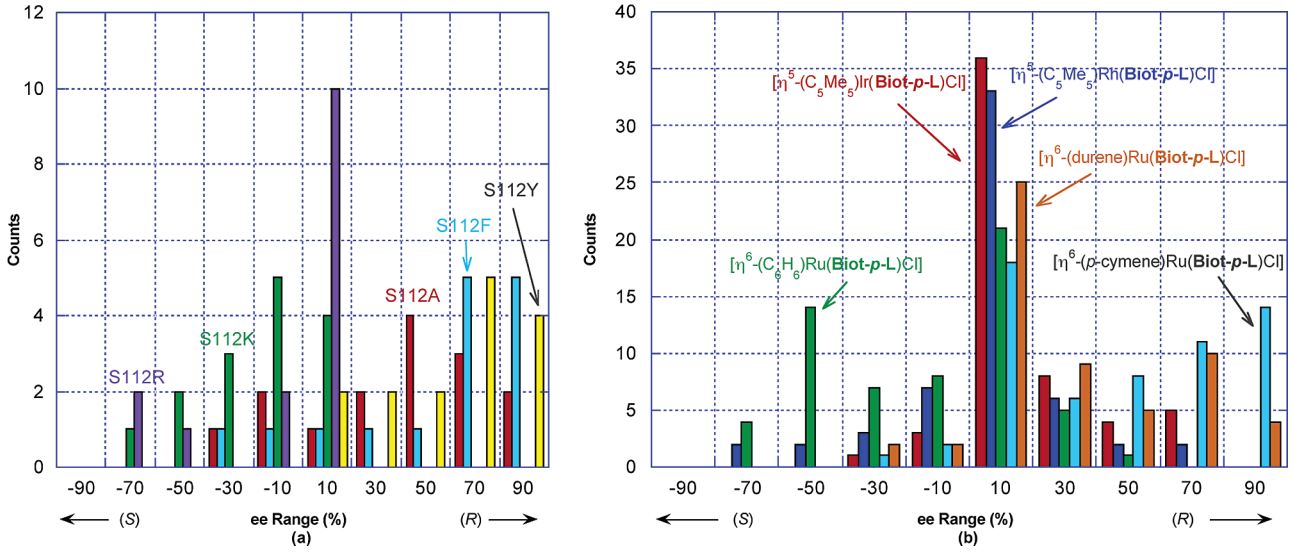

Figure 7. Enantioselectivity histograms as a function of the genetic component (S112X, X = Y, F, A, R, K mutants displayed) (a); and the chemical component (b).

WT Sav and S112T (polar residues); S112E (coordinating residue); S112R (cationic residue) and S112N.

The results of the screening are summarized in a fingerprint format in Figure 8. Numerical data are collected in Table 2. The general features can be summarized as follows:

(i) The selectivity and conversion trends observed for these substrates are similar to those observed with acetophenone derivatives **1a**−**c**: [η^6-(*p*-cymene)Ru(**Biot**−***p*-L**)Cl] and [η^6-(benzene)Ru(**Biot**−***p*-L**)Cl] often yield opposite enantiomers, with better conversions for the former catalyst precursor.

(ii) The dialkyl ketones give poor to modest enantioselectivities (Table 2, entries 1−4).

(iii) For the reduction of 2-acetylpyridine **5** in the presence of a cationic residue at position 112, (i.e., S112R and S112K), both [η^6-(*p*-cymene)Ru(**Biot**−***p*-L**)Cl] and [η^6-(benzene)Ru(**Biot**−***p*-L**)Cl] afford (*S*)-products (51% ee and 70% ee,

Table 1. Selected Conversions and Enantioselectivities Obtained for the Transfer Hydrogenation of Acetophenone Derivatives **1a**−**c** Catalyzed by [η^n-(C_nR_n)M(**Biot**−***p*-L**)Cl] ⊂ S112X[a]

entry	protein	complex	substrate	conv. (%)	ee (%)
1	S112A Sav	[η^6-(*p*-cymene)Ru(**Biot**−***p*-L**)Cl]	**1c**	98	91(*R*)
2	WT Sav	[η^6-(*p*-cymene)Ru(**Biot**−***p*-L**)Cl]	**1c**	86	91(*R*)
3	S112Y Sav	[η^6-(*p*-cymene)Ru(**Biot**−***p*-L**)Cl]	**1a**	95	90(*R*)
4	S112Y Sav	[η^6-(durene)Ru(**Biot**−***p*-L**)Cl]	**1b**	88	92(*R*)
5	S112F Sav	[η^6-(durene)Ru(**Biot**−***p*-L**)Cl]	**1b**	89	83(*R*)
6	S112K Sav	[η^6-(*p*-cymene)Ru(**Biot**−***p*-L**)Cl]	**1a**	64	20(*S*)
7	S112A Sav	[η^6-(benzene)Ru(**Biot**−***p*-L**)Cl]	**1c**	74	41(*R*)
8	S112F Sav	[η^5-(C_5Me_5)Rh(**Biot**−***p*-L**)Cl]	**1b**	73	60(*R*)
9	S112G Sav	[η^5-(C_5Me_5)Rh(**Biot**−***p*-L**)Cl]	**1b**	60	52(*S*)
10	WT Sav	[η^5-(C_5Me_5)Rh(**Biot**−***p*-L**)Cl]	**1b**	48	52(*S*)
11	S112T Sav	[η^6-(benzene)Ru(**Biot**−***p*-L**)Cl]	**1b**	90	55(*S*)
12	S112T Sav	[η^5-(C_5Me_5)Ir(**Biot**−***p*-L**)Cl]	**1b**	95	16(*S*)
13	S112Y Sav	[η^5-(C_5Me_5)Ir(**Biot**−***p*-L**)Cl]	**1b**	96	80(*R*)
14	S112N Sav	[η^6-(*p*-cymene)Ru(**Biot**−***p*-L**)Cl]	**1b**	94	82(*R*)

[a] The catalytic runs were performed at 55 °C for 64 h using the mixed buffer HCO_2Na (0.48 M) + $B(OH)_3$ (0.41 M) + MOPS (0.16 M) at $pH_{initial}$ = 6.25. Ru: substrates **1a**−**c**: formate ratio 1:100: 4000 (i.e. 100 equiv of substrate vs Ru). The results presented here represent the average of at least two catalytic runs.

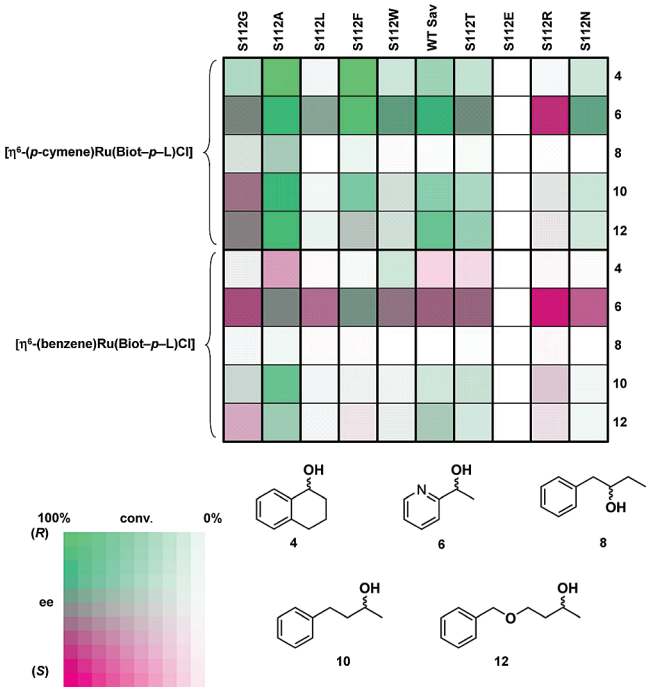

Figure 8. Fingerprint display of the results for the transfer hydrogenation of the aromatic ketones **3** and **5** and the aliphatic ketones **7**, **9**, and **11** in the presence of two biotinylated d^6-piano stool complexes [η^6-(arene)Ru(**Biot**−***p*-L**)Cl] (arene = *p*-cymene, benzene) combined with 10 representative S112X streptavidin isoforms. The catalytic runs were performed with cocktail mixtures of the substrates at 55 °C for 64 h using the mixed buffer HCO_2Na (0.48 M) + $B(OH)_3$ (0.41 M) + MOPS (0.16 M) at $pH_{initial}$ = 6.25. Ru: substrates: formate ratio 1:100: 4000. Please refer to the Supporting Information for a tabulation of all catalytic runs.

respectively, Table 2, entries 5−6). This suggests that the positive charge at this position by-and-large dictates which prochiral face of the basic substrate is presented to the biotinylated piano stool complex.

Mechanistic Considerations. The starting point for this study was the theoretical prediction that, in the related homogeneous catalytic system, both hydrogens are delivered to the prochiral substrate without the substrate binding to the metal.[39,40] In the context of this work, two points are worthy of emphasis:

Table 2. Selected Conversions and Enantioselectivities Obtained for the Transfer Hydrogenation of Ketones **3**, **5**, **7**, **9**, and **11** Catalyzed by [η^6-(arene)Ru(**Biot**−***p*-L**)Cl] ⊂ S112X[a]

entry	protein	complex	substrate	conv. (%)	ee (%)
1	S112A Sav	[η^6-(*p*-cymene)Ru(**Biot**−***p*-L**)Cl]	**11**	97	69(*R*)
2	S112A Sav	[η^6-(*p*-cymene)Ru(**Biot**−***p*-L**)Cl]	**9**	98	48(*R*)
3	S112A Sav	[η^6-(benzene)Ru(**Biot**−***p*-L**)Cl]	**9**	58	52(*R*)
4	S112A Sav	[η^6-(*p*-cymene)Ru(**Biot**−***p*-L**)Cl]	**7**	71	30(*R*)
5	S112R Sav	[η^6-(*p*-cymene)Ru(**Biot**−***p*-L**)Cl]	**5**	94	51(*S*)
6	S112R Sav	[η^6-(benzene)Ru(**Biot**−***p*-L**)Cl]	**5**	95	70(*S*)
7	S112F Sav	[η^6-(*p*-cymene)Ru(**Biot**−***p*-L**)Cl]	**5**	95	76(*R*)
8	S112F Sav	[η^6-(*p*-cymene)Ru(**Biot**−***p*-L**)Cl]	**3**	70	96(*R*)
9	S112Y Sav	[η^6-(*p*-cymene)Ru(**Biot**−***p*-L**)Cl]	**3**	79	97(*R*)
10	S112A Sav	[η^6-(benzene)Ru(**Biot**−***p*-L**)Cl]	**3**	44	51(*S*)

[a] The catalytic runs were performed at 55 °C for 64 h using the mixed buffer HCO_2Na (0.48 M) + $B(OH)_3$ (0.41 M) + MOPS (0.16 M) at $pH_{initial}$ = 6.25. Ru: substrates: formate ratio 1:100: 4000 (i.e. 100 equiv of substrate vs Ru). The results presented here represent the average of at least two catalytic runs.

Scheme 5. Computed Transition-State Structures Leading to Both Enantiomers of the Product (adapted from ref 40)

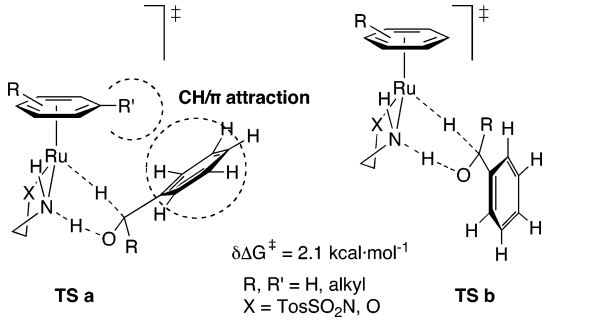

(i) Both hydrogens required for the reduction of the ketone are provided by the coordinatively saturated d^6-piano stool complex: one hydride and one acidic N−H proton from the coordinated amine.

(ii) The computed difference in transition-state energies for the diastereomeric complexes, which ultimately yield both enantiomers of the product, is 2.1 kcal·mol^{-1}. This difference in energy is by-and-large governed by attractive CH/π interactions between the aromatic substrate and the η^6-bound arene. The theoretical study reveals that these CH groups can be either aromatic or pendant aliphatic groups on the η^6-bound arene (Scheme 5).

To test the validity of the involvement of an acidic N−H proton, the *N*-dimethyl analogue **Biot**−***p*-LMe$_2$** was prepared and tested. The catalytic performance of [η^6-(*p*-cymene)Ru(**Biot**−***p*-LMe$_2$**)Cl] ⊂ WT Sav was evaluated: no conversion (<3%) was observed either for the reduction of acetophenone **1a** or 2-acetylpyridine **5**. Introduction of a cationic residue at position S112 (i.e., S112K) does not increase the yield, thus suggesting that the protonation of the substrate indeed requires an acidic proton in the first coordination sphere of the catalyst.

Although the enantioselectivity is mostly governed by the nature of the biotinylated moiety (see Figure 7b), point mutations can, in some cases, lead to an inversion of enantioselectivity. In such cases, we speculate that protein−substrate interactions partially outweigh the dominant CH/π interactions, which favor one diastereomeric transition state over the other. This tendency is particularly pronounced with cationic residues at position S112, which yield preferentially (*S*)-reduction products, irrespective of the biotinylated catalyst (see Figure 7a). This trend

is most prominent for 2-acetylpyridine, which may undergo hydrogen-bonding interactions with the cationic residues at position S112. For the other aromatic substrates, we suggest that cation/π interactions[57] favor **TS b**. In the presence of nonaromatic ketones **7**, **9**, and **11**, there is no clear-cut preference between *Re* or *Si* face reduction as the CH/π attraction is less pronounced or absent. The additional degrees of freedom introduced between the aryl "steric recognition" element and the prochiral ketone do not allow the second coordination sphere interactions to impose an efficient discrimination. As a result, the enantioselectivities for these substrates remain modest. On the basis of these observations, we suggest that the enantioselection mechanism is similar to that proposed by Noyori and co-workers (see Schemes 1 and 5). Although this remains to be demonstrated, we believe that, upon incorporation in the host protein, the nature of the η^n-bound arene by-and-large dictates the absolute configuration of the metal, which, in turn determines the selectivity trends apparent in Figure 7b.

Summary and Outlook

Screening of 21 biotinylated d^6-piano stool complexes [η^n-(C_nR_n)M(**Biot**−***q*-L**)] in the presence of 20 streptavidin isoforms (S112X Sav) for the enantioselective transfer hydrogenation of prochiral substrates has revealed several noteworthy features:

(i) The localization of the biotinylated catalyst, imposed by the aromatic spacer, plays an essential role in determining the activity of the resulting artificial metalloenzyme: only the para-substituted ligand **Biot**−***p*-L** affords significant conversions.

(ii) The Ru-based catalysts outperform both the Rh- and Ir-based systems. This contrasts with a recent report that demonstrated the versatility of a [Cp*Rh]-based catalyst for the enantioselective aqueous transfer hydrogenation of acetophenone derivatives.[36]

(iii) The nature of the η^6-bound arene plays a critical role in the enantioselectivity. Fine-tuning is achieved by saturation mutagenesis at position S112. The highest enantioselectivities are achieved with either aromatic residues (i.e., S112F and S112Y) for (*R*)-products or with cationic residues (i.e., S112R and S112K) for (*S*)-products.

(iv) The presence of a coordinating amino acid residue at position S112 totally shuts off catalytic actvity. This confirms the docking simulations which suggest that this residue lies close to the metal in [η^6-(*p*-cymene)Ru(**Biot**−***p*-L**)H] ⊂ WT Sav.

(v) Good enantioselectivities can be achieved for aromatic ketones (up to 97% ee (*R*) for **4**). Nonaromatic ketones are reduced with modest enantioselectivity (up to 69% ee (*R*) for **12**).

These results suggest that, saturation mutagenesis at a residue close to the computed position of the biotinylated catalyst, combined with chemical variations of the d^6-piano stool moiety, are a powerful tool for the optimization of artificial transfer hydrogenases based on the biotin−avidin technology. Current efforts include the structural characterization of the artificial metalloenzyme as well as the implementation of a high-throughput assay.[58] Such an assay will allow us to fully exploit the potential of directed-evolution methodologies combined with chemical optimization (i.e., chemogenetic[6]) to produce artificial metalloenzymes which unite the best of homogeneous and enzymatic catalysis.

Acknowledgment. We thank Prof. C. R. Cantor for the streptavidin gene as well as Profs. J.-M. Neuhaus and P. Schürmann for their help with protein production. We thank Dr. C. Malan and S. Guerra for the synthesis of **Biot**−***p*-LMe$_2$**. This work was funded by the Swiss National Science Foundation (FN 200021-105192/1), CERC3 (Grant FN20C321-101071), the Roche Foundation, the Canton of Neuchâtel as well as FP6 Marie Curie Research Training Network (IBAAC network, MRTN-CT-2003-505020). We thank Umicore Precious Metals Chemistry for a loan of ruthenium.

Supporting Information Available: Listing of all catalytic runs performed as cocktails, complete experimental procedures, including characterization of intermediates and ligands, and transfer hydrogenation protocol as well as HPLC and GC methods used. This material is available free of charge via the Internet at http://pubs.acs.org.

JA061580O

(57) Schärer, K.; Morgenthaler, M.; Paulini, R.; Obst-Sander, U.; Banner, D. W.; Schlatter, D.; Benz, J.; Stihle, M.; Diederich, F. *Angew. Chem., Int. Ed.* **2005**, *44*, 4400−4404.

(58) Taran, F.; Gauchet, C.; Mohar, B.; Meunier, S.; Valleix, A.; Renard, P. Y.; Créminon, C.; Grassi, J.; Wagner, A.; Mioskowski, C. *Angew. Chem., Int. Ed.* **2002**, *41*, 124−127.